Clays and Clay Minerals, Vol. 46, No. 4, 400–413, 1998.

HISINGERITE: A FERRIC KAOLIN MINERAL WITH CURVED MORPHOLOGY

RICHARD A. EGGLETON AND DAVID B. TILLEY

Cooperative Research Centre for Landscape Evolution and Mineral Exploration, Department of Geology, Australian National University, Canberra, ACT 0200 Australia

Abstract—Hisingerite, first described in 1810, has been variously regarded as noncrystalline, as a septechlorite, as ferric allophane, as ferric halloysite and as poorly crystalline nontronite. Hisingerite from the original localities of Gillinge and Riddarhyttan in Sweden has a composition close to $Fe_2O_3 \cdot 2SiO_2 \cdot 2H_2O$. X-ray diffraction (XRD) analysis of Riddarhyttan hisingerite yields very broad maxima at 7.7, 4.44, 3.57, 2.56, 2.26, 1.69 and 1.54 Å, and that from Gillinge is similar. Cation exchange capacities are 2.2 meq/100 g (Riddarhyttan) and zero (Gillinge). Transmission electron microscopy (TEM) shows a fabric of concentric spheres and part spheres, with diameters of about 140 Å and walls up to six 7-Å layers thick. High-resolution images of the sphere walls reveal a 2-layer structure similar to that of kaolinite. A calculated diffraction pattern based on a model of 4 concentric shells of ferric kaolinite structure matches the observed pattern quite closely. Some other hisingerites, notably that from Bellevue King Mine, Idaho, show 10-Å layers as well as 7-Å layers, and this hisingerite has a CEC of 32 meq/100 g and a weak 15.5-Å X-ray reflection in addition to a pattern similar to Riddarhyttan hisingerite. It is concluded that hisingerite is a curved ferric 7-Å 1:1 layer silicate analogous to halloysite, and that many of the hisingerites reported in the literature contain admixed nontronite.

Key Words—Cation Exchange Capacity, Halloysite, Hisingerite, Kaolinite, Nontronite, Transmission Electron Microscopy, X-ray Powder Diffraction.

INTRODUCTION

The mineral now known as hisingerite was first described by Hisinger (1810) in a paper entitled "Svart Stenart från Gillinge Jern-Grufva i Södermanland" (Black species of stone from Gillinge Jern-Grufva in Södermanland). Berzelius (1819) named this mineral "hisingerit", whereas Hisinger (1826) called the Gillinge mineral "gillingit". In 1828 Hisinger published a report on material from Riddarhyttan under the title: "Analysis of the iron silicate with the attributed name Hisingerit". He described the Riddarhyttan specimen as formless; black; with uneven, imperfectly developed, lustrous fracture; brittle; not particularly dense; and brown-yellow in powder form. Hisinger's analysis yielded 36.30% SiO_2, 44.39% Fe_2O_3 and 20.7% H_2O, which corresponds closely to $Fe_2O_3 \cdot 2SiO_2 \cdot 2H_2O$. A second, smaller sample from Bodenmais, he said, was by and large the same, and von Kobell (1828) agreed on the basis of his analysis of Bodenmais material (known until then as "thraulite"). Hisinger did not refer to the Gillinge sample in his 1828 paper. In 1839, Mohs considered both the Riddarhyttan and Gillinge samples to be hisingerite, as did Rammelsberg in 1848, and most later publications have regarded gillingite as a variety of hisingerite.

Samples with similar modes of occurrence and similar physical, optical and chemical properties were discovered over the following century (Table 1). The common feature of these records is that hisingerite is described as being brown to black with a resinous lustre, as brittle with a conchoidal fracture and as having a Mohs hardness of between 3 and 3.5. Twentieth-century improvements in analytical precision and the introduction of XRD, infrared (IR) spectroscopy and thermogravimetric analysis (TGA) provided additional properties for hisingerite, but did little to clarify its nature. Hawkins and Shannon (1924) described birefringent material associated with hisingerite from the Brandywine Quarry in Delaware, which they named "canbyite", concluding that this was the crystalline compound corresponding to the amorphous hisingerite. Also in 1924, Schwartz described similar material from Parry Sound, Ontario, Canada, comprising both birefringent and isotropic phases. Hewett and Schaller (1925) reported hisingerite from the Minnie Moore and Bellevue King Mines in Blaine County, Idaho, and analyzed the latter.

Gordon (1944) briefly described 2 hisingerites from the tin mines of Cerro de Llallagua, Bolivia. There is insufficient description of the materials to be absolutely confident that the samples are pure. The analysis of a sample from Chojnacota conforms to other hisingerites, whereas that from Llallagua is much higher in iron; its dark brown color, high refractive index and iron content suggest included iron oxides. Only the Chojnacota specimen is included in Table 1.

The first report of XRD analysis of hisingerite appears to be that of Gruner (1935), who found 3 broad peaks centered at 4.4, 2.6 and 1.5 Å, and these have been recorded in all subsequent experiments. Bowie (1955) found additional lines at 3.55 and 1.7 Å in all

but 1 of the 6 hisingerites he examined, and Whelan and Goldich (1961) reported a further line at 7.5 Å in a sample from the E Mesabi Range, as well as XRD results for 2 hisingerites from Beaver Bay, Minnesota, previously described as "chlorophaeite" by Muir (1954).

Kohyama and Sudo (1975) described a mineral in clayey volcanic rock fragments that was deep green to blue in color, and which altered in color on exposure first to black, then to brown. The diffraction pattern and composition of this material match those of poorly crystalline nontronite, and the electron micrographs are described as showing thin flakes with a smectite-like shape. Kohyama and Sudo (1975) chose to identify this sample as hisingerite, thus appearing to establish that hisingerite is poorly crystalline nontronite. An alternate interpretation is that their sample is poorly crystalline nontronite.

Eggleton et al. (1983) examined 2 so-called hisingerites and 3 "sturtites" (Mn-hisingerite or Fe-neotocite) from Broken Hill, New South Wales, Australia, concluding that hisingerite was noncrystalline and composed of a mass of joined spheres ranging from 50–100 Å in diameter. The outer shell of the spheres showed evidence of a rudimentary layer structure. Shayan (1984) described hisingerite from a basalt quarry near Geelong, Victoria, Australia. It had a cation exchange capacity (CEC) of 68.6 meq/100 g. Electron micrographs show a fabric of "spherical onion structures", ranging from 140–200 Å in diameter, which appear to be composed of layers; interlayer spacings of 4.5, 9, 11 and 13.6 Å were reported. Eggleton (1987) further examined this specimen, finding concentric lattice fringes at 3-Å spacings parallel to the sphere walls.

Manceau et al. (1995) examined a brown-black scale deposit from the Salton Sea geothermal field. In addition to the properties listed in Table 1, they report an XRD pattern similar to nontronite, having a 17.7-Å line in addition to the normal peaks of hisingerite. They concluded that their sample, because it had an XRD pattern similar to hisingerite (though not conforming to published hisingerite chemistry, and including a 17.7-Å XRD line not previously reported for hisingerite), should be identified as hisingerite, and then concluded that hisingerite is a poorly crystallized, non-stoichiometric nontronite. Many of the hisingerite samples in the literature are reported to contain impurities, and such analyses have not been considered in summarizing literature compositions.

Most authors have attempted to classify hisingerite within the known families of silicates. Sustschinsky (1910) suggested it belonged in the group of iron septechlorites, and Simpson (1919) considered hisingerite to be the ferric homologue of halloysite. Gruner (1935) wrote: "Hisingerite appears to be amorphous. It gives about 5 broad indistinct bands (XRD) which agree with most lines of nontronite except for line number 1 (of nontronite) which could not be identified with nontronite." MacEwan (1951) appears to have begun the trend toward regarding hisingerite as nontronite. In the first edition of "X-ray identification and crystal structure of clay minerals", he mentions hisingerite under obsolete names for montmorillonite minerals, suggesting, on the basis of Gruner's data, that hisingerite may be a less well-crystallized variant (of nontronite). Sudo and Nakamura (1952) concluded that hisingerite is a gel mineral like allophane. Bowie (1955) mentions nontronite as having a similar diffraction pattern, and suggested using the presence or absence of a 14-Å line to distinguish nontronite from hisingerite. Whelan and Goldich (1961) concluded that hisingerite "might easily be a mixture of two or more minerals". They suggest that the sample they examined might have formed as an alteration product of ferrous saponite. By 1961, MacEwan regarded "amorphous" as "a term which should perhaps be interpreted as very finely crystalline". Thus, the distinction between nontronite and hisingerite was gradually eroded. Mackenzie and Berezowski (1980) concluded that "hisingerites contain elements of poorly crystalline structure with similar characteristics to nontronite". Brigatti (1981) found, from an examination of the chemical compositions of smectites and hisingerite, that by assuming the tetrahedral site was occupied, on average, by $[Si_{3.3}Fe_{0.7}]$, the analyses of hisingerite corresponded to a nontronite formula, and thus it was a member of the smectite group. Most recently, Manceau et al. (1995) concluded that hisingerite was poorly crystallized, non-stoichiometric nontronite.

Hisingerite's reported physical and chemical properties are unlike those of most clay minerals, and particularly unlike those of nontronite. Nontronite has a hardness of 1 and a dull or earthy luster, hisingerite a hardness of about 3, with a vitreous to resinous luster. Hisingerite has an octahedral : tetrahedral cation ratio close to 1:1, and contains little aluminium, whereas nontronite has a ratio of 1:2, and commonly contains aluminium. These properties of nontronite would not be expected to vanish just because the mineral is poorly crystallized.

Some of the confusion may have arisen from too ready acceptance that a ferric silicate with very broad diffraction maxima and absent or suppressed 15-Å reflection must be hisingerite. Study of the published record suggests that at least 2 materials have been called "hisingerite". Hisinger's analyzed material from Riddarhyttan is certainly hisingerite, and the sample from Gillinge has been equally regarded as hisingerite. Other samples are only hisingerite if they are the same, or very similar. In this paper we reexamine type hisingerite from Riddarhyttan and the earlier Gillinge material using XRD, chemical analysis, CEC measurements and high-resolution transmission elec-

Table 1. Literature source, localities and physical properties of hisingerite samples.

Date	Author	Locality	Fracture	Color	Luster	Streak
1810	Hisinger	Gillinge		black		
1828	Hisinger	Riddarhyttan	conchoidal†	dark brown†	vitreous†	brown-yellow†
1870	Church	Cornwall	conchoidal	dark brown		pale rust brown
1919	Simpson	Westonia	conchoidal	brownish-black	resinous	nr
1924	Hawkins & Shannon	Canbyite		dark brown		
1924	Schwartz	Parry Sound	brittle‡	black‡	resinous‡	yellow
1925	Hewett & Schaller	Bellevue King		fresh: red, changes to black, then dark brown	vitreous-greasy	yellowish brown
1944	Gordon	Chojnacota	nr	reddish and brownish	gum-like	orange rufous
1950	Osborne & Archambault	Montaubon-les-Mines	conchoidal	black	vitreous-resinous	pale yellow
1952	Sudo & Nakamura	Kawayama		dark green turning dark brown, or dark brown	somewhat vitreous	nr
1955	Bowie #1	Nicholson		dark brown-black	greasy-vitreous	nr
1961	Dietrich	Tjolling	conchoidal	dark brown to black	waxy to subvitreous	olive green to greenish brown
1961	Whelan & Goldich	Beaver Bay #1		reddish brown		
1961	Whelan & Goldich	Beaver Bay #2		reddish brown		
1961	Whelan & Goldich	E Mesabi	brittle	black	resinous	nr
1983	Eggleton S1	Broken Hill	conchoidal	blackish brown	vitreous	nr
1983	Eggleton S2	Broken Hill	conchoidal	blackish brown	vitreous	nr
1984	Shayan	Geelong	conchoidal	black	vitreous	green-gray
1995	Manceau et al.	Salton Sea	conchoidal	black	vitreous	
1998	This study	Gillinge 070080	conchoidal	black-brown	subvitreous	brown

† Data determined in this study.
‡ Data from Whelan and Goldich (1961) on a sample provided by Schwartz.

tron microscopy (HRTEM), and compare these with several other "hisingerites", in an effort to resolve or explain the diversity of view as to its nature. We will show that Riddarhyttan and Gillinge hisingerite are almost identical in composition and structure; that they are, in Simpson's words, the homologue of halloysite; and that some other hisingerites contain admixed smectite, probably nontronite.

MATERIALS AND METHODS

The Swedish Museum of Natural History (SMNH) provided "a Berzelius specimen from Gillinge (070080) and a Hisinger specimen from Riddarhyttan (23:0455)", but were unable to verify that these were the materials actually analyzed by Hisinger. Material said to be from Solberg (Lindqvist and Jansson 1962, sample S4 University of Uppsala MGUI 400/2), and a second specimen from Gillinge, number 48-1817, were also provided. This study has raised doubts about the source of sample MGIU 400/2; in this paper we refer to it as "Solberg". The Smithsonian National Museum of Natural History (SNMNH), USA, provided samples from Canby (94715, Hawkins and Shannon, 1924) and Bellevue King (1028901, Hewett and Schaller, 1925). Sample S1 of Eggleton et al. (1983) from Broken Hill, NSW, was also reexamined. The Riddarhyttan sample comprised a core of hisingerite about 3 × 2 cm, with a cover of pyrite and pyrrhotite. Sample 070080 from Gillinge appeared uniform to visual inspection, but on light crushing was found to contain calcite, magnetite, almandine and amphibole. Sample 48-1817 from Gillinge contains small domains of resinous brown hisingerite mixed with calcite and chlorite. "Solberg" material is manganiferous and contains magnetite and calcite with a trace of a well-crystallized 7-Å layer silicate, and the sample from Canby contains calcite. Visual inspection, hand picking and heavy liquid and magnetic separation were used to purify the samples for detailed study.

Samples for XRD were crushed and mounted on a low-background quartz plate, then scanned for 15 h from 4 to 80 °2θ in a Siemens D501 θ/2θ goniometer using Cu$K\alpha$ radiation (40 kV, 25 mA) and a post-sample graphite monochromator. A second very slow scan from 2 to 15 °2θ was run on a Siemens Type F diffractometer using Co$K\alpha$ radiation. TEM specimens

https://doi.org/10.1346/CCMN.1998.0460404 Published online by Cambridge University Press

Table 1. Extended.

H	SG	Optics	RI
	3.045		
3.5†	2.35†	iso/aniso	1.57–1.58†
2.75	1.74		
	2.27	iso/aniso	
		aniso	1.552–1.595
2.5‡	2.5	iso/aniso	1.50–1.56
3.5	nr	isotropic	1.57
	2.475	isotropic	1.57
2.5	2.53–2.55	isotropic	1.61 fresh 1.51 stored
		iso/aniso	
3.5	2.32–2.64	iso/aniso	1.584–1.621
3–3.5	1.786	iso/aniso	1.47–1.486
		aniso	
		aniso	
3	2.67	isotropic	1.66
3			
3			
		isotropic	
3.5			

were prepared by deposition from alcohol onto holey carbon grids and examined in a JEOL 200CX microscope operating at 200 kV, with top-entry non-tilting stage. Electron microprobe (EMP) analyses were performed on polished grains using an EDS JEOL 6400 SEM equipped with a thin window detector, operating at 15 kV. Analyses, including analyses for oxygen, were reported as atom% but recalculated for Table 2 as oxide wt%. Water and carbon dioxide were measured using a LECO gas analyzer, heating rate 1°/s, on samples that had been dried for 2 h at 100 °C, and repeated on air-dried material for the Riddarhyttan sample. The distribution of carbonate was investigated by laser Raman spectral analysis of 2-μm areas, and the behavior of water during heating studied by IR emission spectrometry. CEC was measured by determining exchangeable Ba by X-ray fluorescence (XRF) analysis (Churchman et al. 1994). The sample from Riddarhyttan was analyzed by XRF, and for Fe(II) by titration, in the INAX Laboratories of the Australian National University (B. W. Chappell, analyst).

RESULTS

Physical Properties

The physical properties of the samples are included in Table 1. Particular attention was paid to the behavior of hisingerite samples in water. Neither by simple immersion nor by grinding underwater did any of the samples examined become plastic or malleable. The density of hisingerite, generally reported to be between 2.2 and 2.6 g/mL, is confirmed in this study for Riddarhyttan hisingerite, with a measured density by Archimedes's method (Archimedes ca. 250 BC) of 2.35. Other samples were insufficiently pure or of insufficient size for density determination.

Composition

The average of 24 analyses in the literature yields a composition for hisingerite close to that of a 1:1 dioctahedral layer silicate, with 18 having Si:(Al + Fe + Mn + Mg) between 1:0.9 and 1:1.1. If Al is assumed to be tetrahedral and Fe, Mn and Mg octahedral, the tetrahedral : octahedral ratio averages 1:0.9. The new EMP analyses reported here in Tables 2 and 3, and the earlier analyses reported in Table 3, show that, for the samples from Riddarhyttan and Gillinge, Si:(Al + Fe + Mn + Mg) = 1:0.98, or (Si + Al):(Fe + Mn + Mg) = 1:0.96.

Water analyses for hisingerite show considerable variation, partly because it readily adsorbs water from the atmosphere. The results presented here with the EMP data are from material dried at 100 °C for 2 h and then immediately analyzed. All samples show 3 maxima of water loss with increasing temperature (Figure 1). The major loss occurs at 125 °C, amounting to between 4 and 9 wt%. Smaller losses are found at approximately 230 and 330 °C, with water loss continuing up to about 750 °C. The total water lost after the 125 °C maximum is 6.7 ± 0.5%. Published differential thermal analysis (DTA) results from hisingerite show endotherms at 100 °C and from 310 to 380 °C, which correlate to some extent with the 2 main temperatures of water loss at 125 and 330 °C.

The low totals for the EMP analyses probably result from problems with the water analyses. If the probe vacuum and electron beam heating cause less evaporation than occurred during the 2-h drying at 100 °C prior to water analysis, the total water value to be applied to the probe analyses would increase. Support for this interpretation comes from the Riddarhyttan XRF analyses, for which H_2O^+ and H_2O^- were measured on the analytical sample without prior drying. Hisingerite adsorbs water from the atmosphere readily, and variations in ambient humidity may have affected all the H_2O measurements.

Despite careful purification, all bulk samples of hisingerite contain CO_2, reaching 7.7% in the calcite-containing Canby sample. To check the nature of the distribution of carbonate, the polished blocks used in the EMP analyses were examined by reflectance microscopy and subjected to Laser Raman spectroscopy, a technique very sensitive to the presence of carbonate. Hisingerite areas of 2 μm diameter were analyzed

https://doi.org/10.1346/CCMN.1998.0460404 Published online by Cambridge University Press

Table 2. New chemical analyses of hisingerite.

Locality:	Riddarhyttan	Riddarhyttan	Riddarhyttan	Gillinge	"Solberg"	Broken Hill	Canby	Bellevue King
Technique	EMP	XRF	XRF corr†	EMP	EMP	EMP	EMP	EMP
SiO_2	35.83	35.52	36.59	36.98	38.78	36.63	37.62	38.97
Al_2O_3	0.56	0.74	0.76	0.05	0.83	0.96	1.46	1.91
Fe_2O_3	44.08	41.96	43.23	40.57	20.69	39.23	40.79	33.80
FeO	0.00	0.84		0.00	0.00	0.00		
MnO	0.10	0.16	0.17	2.63	22.09	3.56	0.35	1.83
MgO	0.75	0.75	0.77	2.27	3.05	0.35	1.52	2.11
CaO	0.44	0.50		1.07	0.65	0.18	0.57	1.08
Na_2O	0.21	0.01	0.01	0.20	0.08	0.95	0.37	0.10
SO_3		0.77						
CO_2		0.86						
H_2O^+	12.39	13.05	13.44	12.24	10.97	10.05	19.01	14.67
H_2O^-		6.25	6.44					
	94.36	101.41	101.41	96.02	97.13	91.91	101.70	94.46
Structural formulae to +14								
Si	2.03		2.05	2.05	2.01	2.06	2.08	2.18
Al	0.04		0.05	0.00	0.05	0.06	0.10	0.13
Fe(III)	1.88		1.83	1.69	0.81	1.66	1.70	1.43
Fe(II)	0.00		0.00	0.00	0.00	0.00	0.00	0.00
Mn	0.00		0.01	0.12	0.97	0.17	0.02	0.09
Mg	0.06		0.06	0.19	0.24	0.03	0.12	0.18
Ca	0.03		0.00	0.06	0.04	0.01	0.03	0.06
	0.02		0.00	0.02	0.01	0.10	0.04	0.01
OH	4.68		5.04	4.52	3.80	3.78	7.02	5.49
ΣR	1.98		1.95	2.00	2.06	1.93	1.93	1.83
CEC	2.2		2.2	0.0	0.4	10.5	nd	32.5

† "XRF corr" is the data from Column 2 corrected by the subtraction of Fe(II) and SO_3 as pyrite, Ca as calcite and remaining Fe(II) as siderite. This procedure accounted for 0.9% CO_2, which may be compared to the analytical CO_2 figure of 0.86%.

Table 3. Analyses of Gillinge/Solberg hisingerite.

Locality:	Gillinge	Gillinge	Gillinge	Gillinge	Gillinge	Solberg	"Solberg"
Reference	This work	This work	Hisinger	Rammels-berg	M&B	L&J and M&B	This work
Sample number	70080	48-1817			MGIU 400/4	MGIU 400/2	MGIU 400/2
SiO_2	36.98	39.01	27.5	32.18	34.21	35.24	38.78
Al_2O_3	0.05	2.92	5.5	0	0.97	2.00	0.83
Fe_2O_3	40.57	36.38	51.5	30.1	18.68	35.51	20.69
FeO	nd	nd	0	8.63	1.55	2.40	0
MnO	2.63	2.92	0.8	0	20.74	0.34	22.09
MgO	2.27	2.19	0	4.22	3.22	3.77	3.05
CaO	1.07	0.45	0	5.50	1.06	1.99	0.65
H_2O^+	12.24	15.00	11.75	19.37	9.13	10.42	10.97
H_2O^-					9.53	9.03	
	96.02	98.87	97.05	100	99.09	100.7	97.06
to +14	to +14	to +14	to Si=2	to +14	to +14	to +14	to +14
Si	2.05	2.08	2	2.01	1.94	2.02	2.01
Al	0	0.18	0.48	0	0.06	0.14	0.05
Fe(III)	1.69	1.46	2.82	1.42	0.80	1.53	0.81
Fe(II)	nd	nd	nd	0.45	0.08	0.11	0.00
Mn	0.12	0.13	0.04	0	0.99	0.02	0.97
Mg	0.19	0.18	0	0.39	0.27	0.32	0.24
Impurities	magnetite calcite almandine	chlorite calcite		chlorite	magnetite pyrite	chlorite hematite	magnetite calcite 7-Å line

https://doi.org/10.1346/CCMN.1998.0460404 Published online by Cambridge University Press

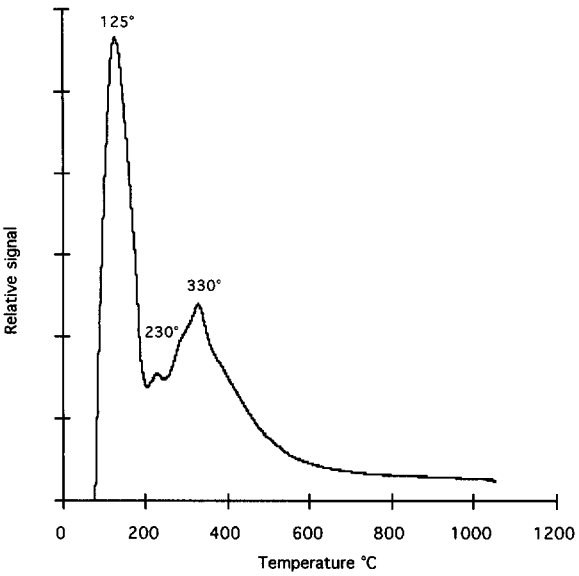

Figure 1. Water evolution relation for Riddarhyttan hisingerite.

(Riddarhyttan, Gillinge, "Solberg" and Broken Hill S1), and yielded no carbonate signal except when macroscopic carbonate was examined.

The structural formulae of Table 2 are all calculated to a charge of 14, that is, to kaolinite stoichiometry. All show slightly more Si and slightly fewer total octahedral cations than an ideal 1:1 layer silicate. The sample from the Bellevue King Mine has a particularly low octahedral cation total and high silicon.

TEM

The dominant feature of the TEM images of all samples is the presence of spheres, part-spheres, and curved aggregates (Figures 2–5). Some regions, particularly near the thin edge of the sample, show nearly complete spheres with concentric layers. Among the spheres are shapes suggestive of part-spheres (caps), irregularly curved segments and almost straight sections. The outer diameter of the more regular spheres ranges between 120 and 200 Å, with the minimum observed diameter of the innermost shell of a concentric sphere being 60 Å. Spheres or part-spheres contain up to 6 concentric shells.

All samples of hisingerite become damaged under the influence of the electron beam. Two or 3 through-focal series images were obtainable at lower magnifications (110,000, 240,000×), but no usable images were obtained at higher magnification. The highest-resolution images obtained show that the concentric shells are 7 Å apart, and that each layer is composed of 2 sheets (Figures 2–5). Fringes perpendicular to the 7-Å layer spacing were imaged at 4.5 Å (Figures 2, 4 and 5).

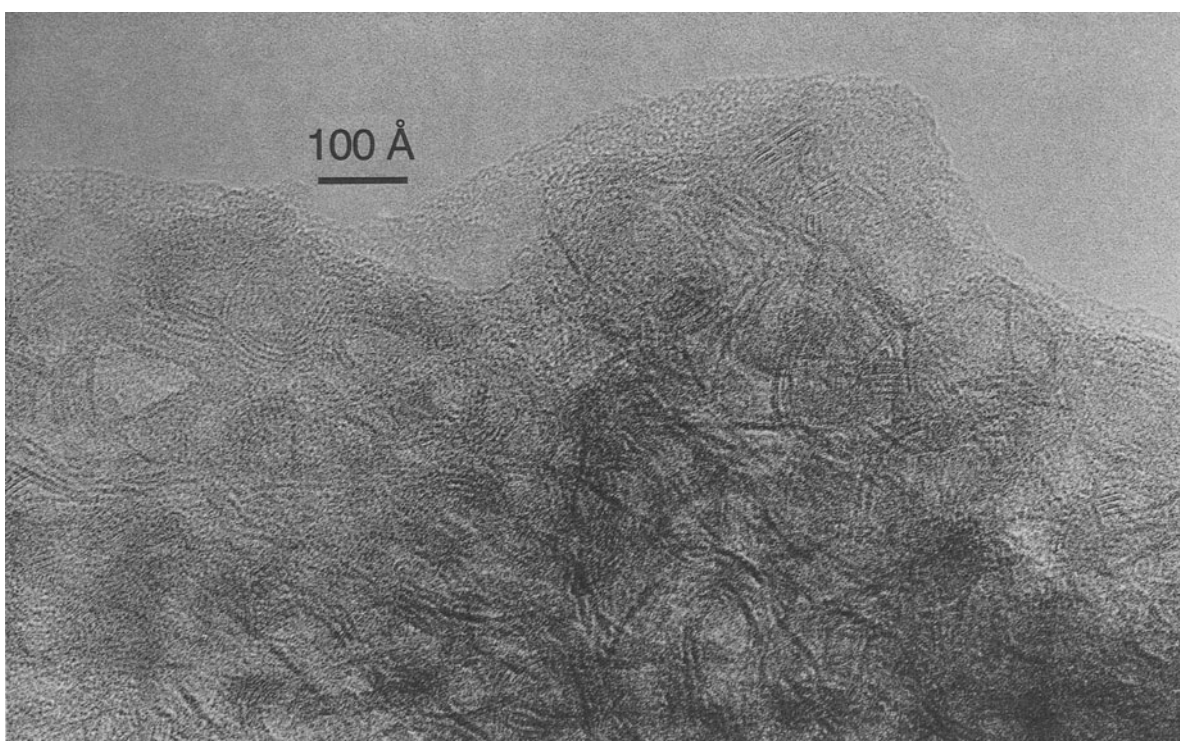

Figure 2. TEM image of Riddarhyttan hisingerite sample SMNH 23:0455.

https://doi.org/10.1346/CCMN.1998.0460404 Published online by Cambridge University Press

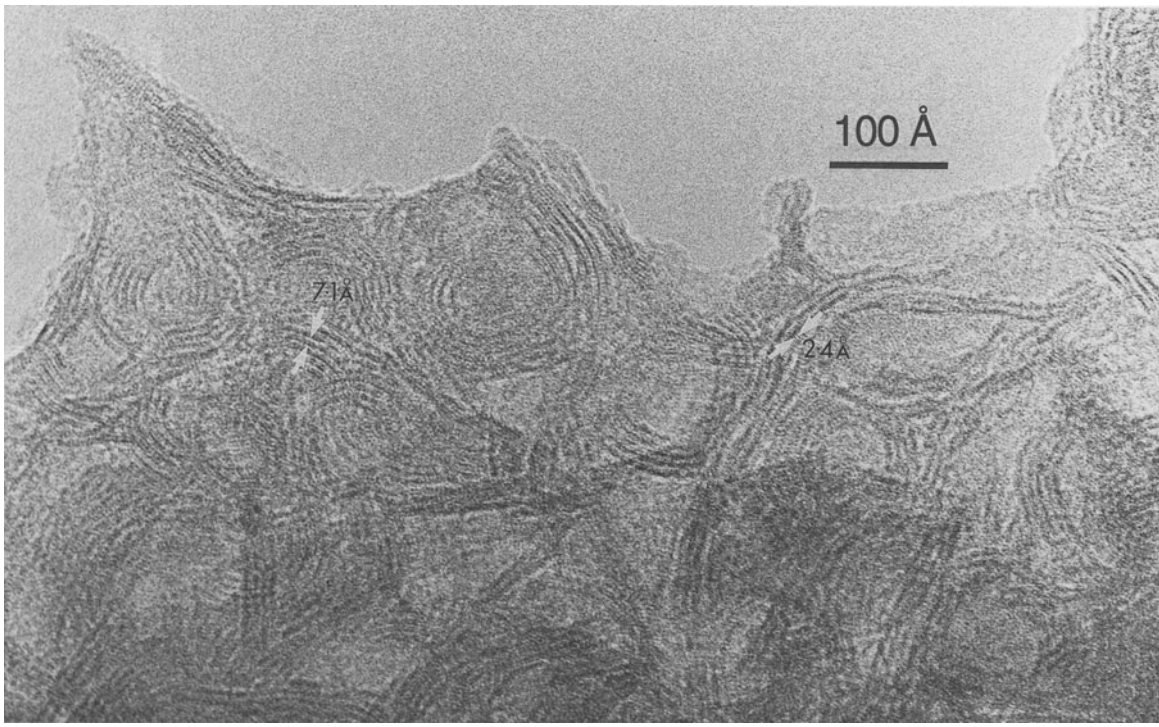

Figure 3. TEM image of Gillinge hisingerite sample SMNH 070080.

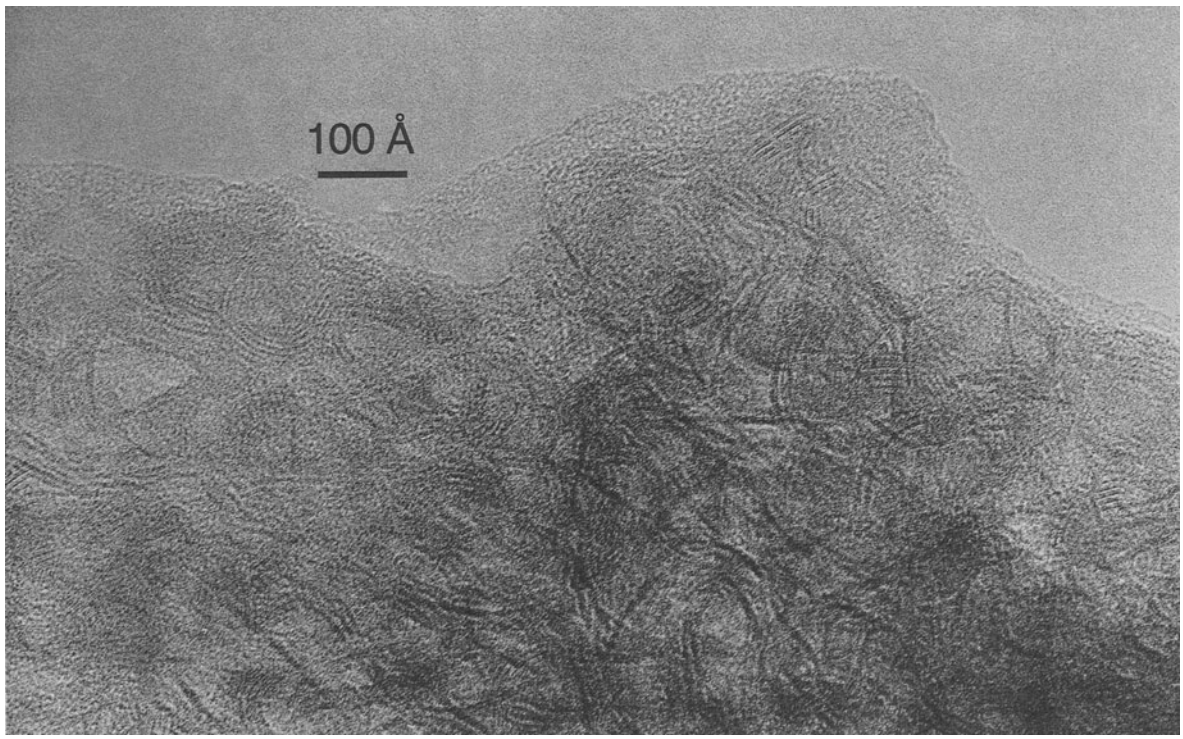

Figure 4. TEM image of "Solberg" hisingerite sample MGIU 400/2.

https://doi.org/10.1346/CCMN.1998.0460404 Published online by Cambridge University Press

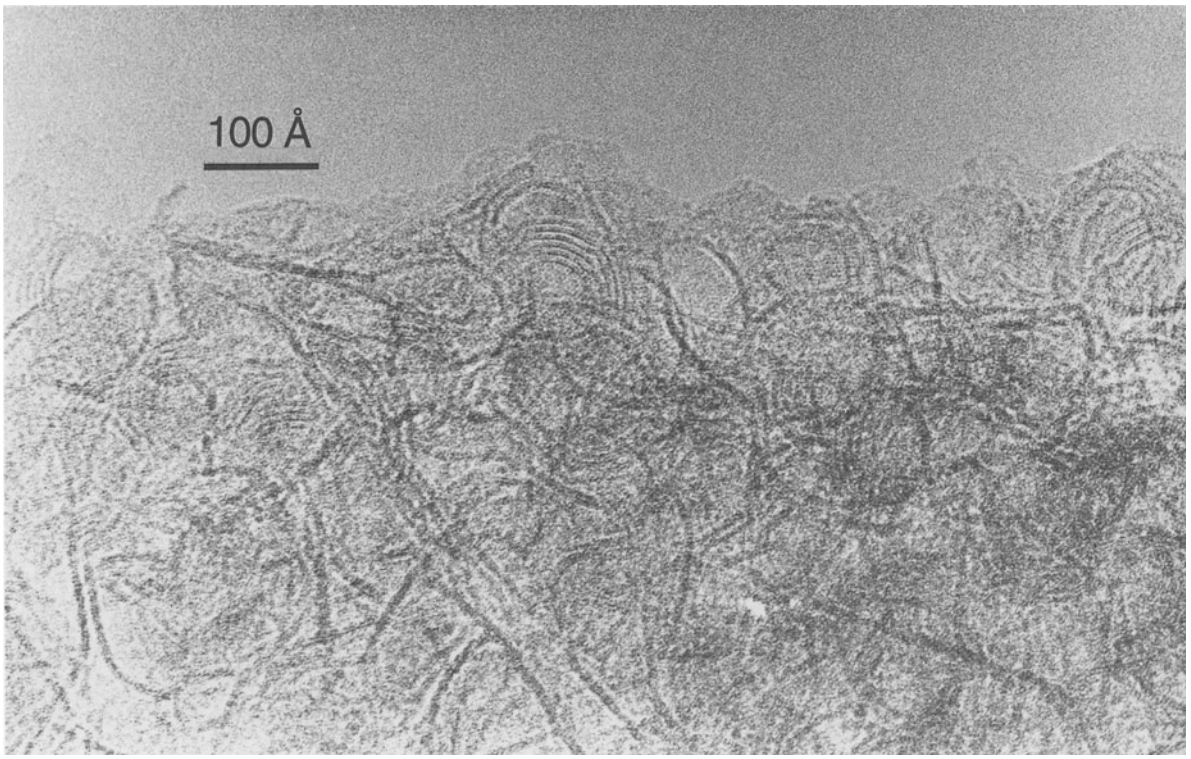

Figure 5. TEM image of Broken Hill hisingerite sample S1.

The samples from the Bellevue King Mine and Canby show, in addition to spheres and curved aggregates (Figure 6a), prominent straighter layers, similar to images of kaolinite and smectite. Some lattice images from this material show a 2-sheet 7-Å spacing and others a 3-sheet 10-Å spacing (Figure 6b). Calculated [001] structure images for ferric-kaolin compare with the experimental 3-sheet images and those for nontronite compare with the 2-sheet images.

XRD

The XRD scans from the 7 samples examined are shown in Figure 7 and summarized in Table 4; they conform to previously reported data, except that the Riddarhyttan and Gillinge samples have distinct, broad peaks at about 7.4 Å, of very weak intensity. All the peaks are weak, typically recording 100 cps, which may be compared with the 02,11 peak of halloysite (1000 cps), and the 001 of oriented kaolinite (15,000 cps).

Of the 7 samples examined, only 2 (Canby and Bellevue King) show any evidence of scattering in the 15-Å region, and this evidence is no more than a slight elevation of the background in the region between 4 and 8°. The others show a smooth decrease in intensity from 2 to 8 °2θ with no indication of scattering in the 001 region for a smectite. Saturation of the Riddarhyttan sample with ethylene glycol and an attempt at formamide intercalation had no detectable effect on the XRD pattern.

CEC

CECs for 5 of the 6 samples examined are included in Table 3. For the Riddarhyttan and Gillinge samples, the CECs are close to zero. Bellevue King hisingerite has a notably higher CEC. Figure 8 shows the CEC for these samples plotted against Al per formula unit. Also plotted is the Geelong hisingerite of Shayan (1984), and sample S4 from Lindqvist and Jansson (1962), the only other specimens in the literature to have composition and CEC reported.

Model Structure

The TEM data show that hisingerite has a strongly curved morphology. There is therefore no lattice to this mineral as a lattice is normally defined. Instead, structural units repeat over the surface of a sphere much as the carbon rings do in fullerenes. At various points on the surface of the sphere, non-hexagonal linkages must occur to accommodate the curvature. It is therefore not possible to calculate an XRD pattern based on Bragg diffraction concepts, nor to describe a unit cell except in the simplest form. Unit cell dimensions a, b and $d(001)$ can be included, and the cell angle γ, but the angles α and β cannot be determined,

https://doi.org/10.1346/CCMN.1998.0460404 Published online by Cambridge University Press

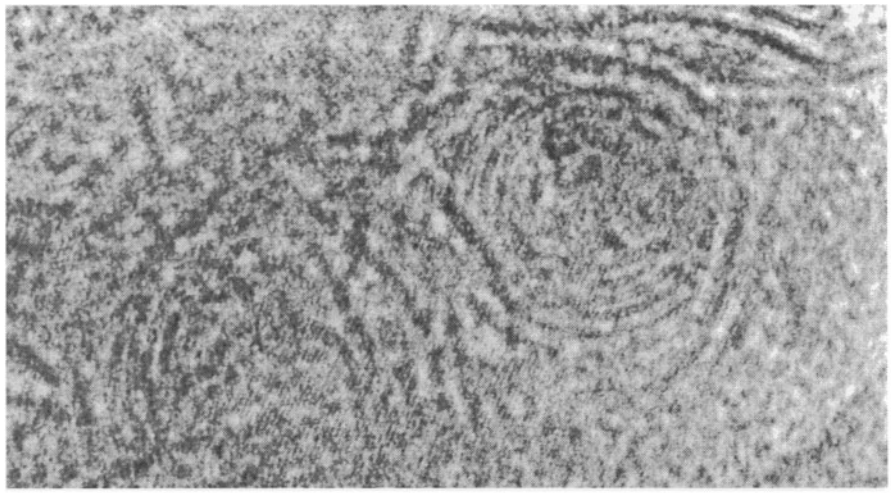

a)

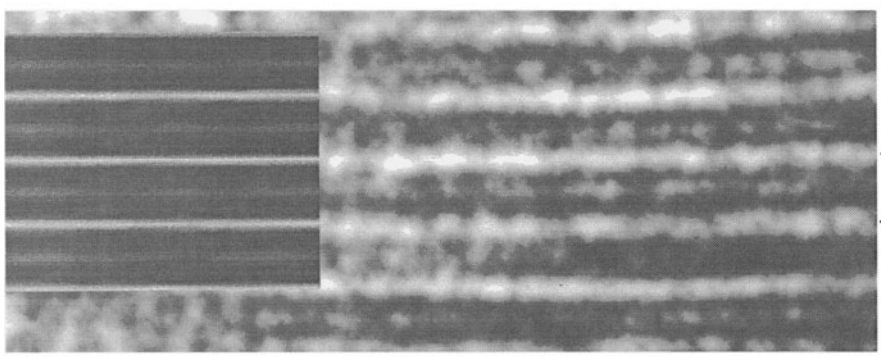

b)

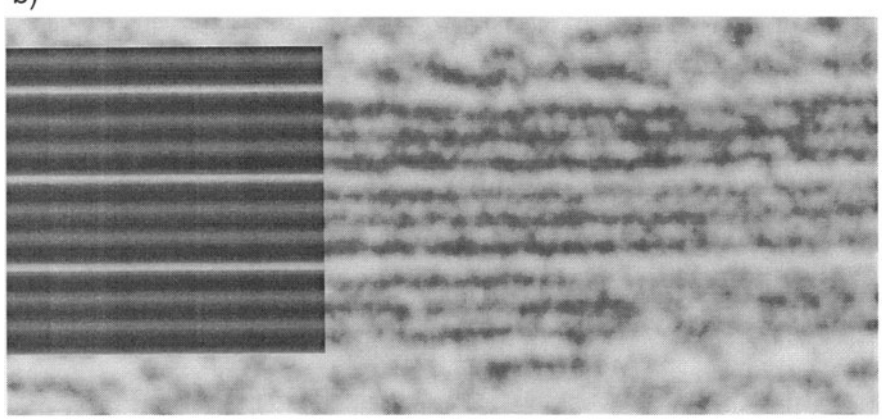

c)

Figure 6. TEM images of a) spherical hisingerite, b) platy hisingerite and c) nontronite from Canby: SNMNH 1028901, with calculated [001] TEM images at 50 nm underfocus.

https://doi.org/10.1346/CCMN.1998.0460404 Published online by Cambridge University Press

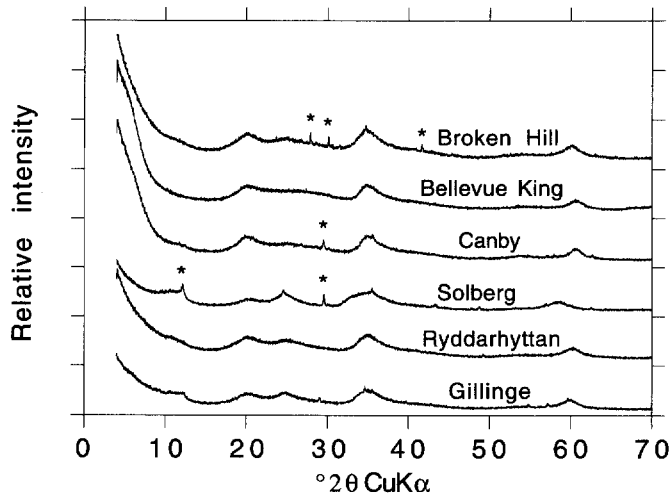

Figure 7. XRD scans for hisingerites (Cu$K\alpha$). Peaks marked with a star (*) are from impure minerals, mostly calcite. Intensity scale is for the lowest trace; under the same experimental conditions, the 3.34-Å peak of quartz and the 001 peak of an oriented aggregate of kaolinite both have peak intensities of about 15,000 cps.

since these will vary from unit cell to unit cell along the surface of the spherical shell (Figure 9).

Nonetheless, within 1 unit cell, α and β can be defined in order to locate atomic positions. Cowley (1961) suggested that curved crystals, such as are found in serpentines, had small domains of XRD coherence. The clearest TEM images of hisingerite (such as Figures 2, 4 and 5) show discontinuities in curvature within individual spheres, supporting Cowley's interpretation. On this basis, intensities were calculated for a model constructed as a spherical cap of diameter 80 Å with a radius of curvature of 70 Å (Figure 10), built from kaolin-like unit cells but with Fe in place of Al (Table 5). In order to best model the position and relative intensities in the 002 and 020 regions, the *b*- and *c*-axes and the *z*-coordinates were adjusted a small amount by trial and error, leading to parameters: a = 5.37 Å, b = 9.3 Å, $d(001)$ = 7.03 Å, with atom planes at Fe = 0.0 Å, octahedral anions (O,OH) at 1.12 Å, silicons at 2.81 Å, basal oxygens (Ob) at 3.44 Å. The comparable figures for kaolinite are Al:0.0 Å, (O,OH):1.14 Å, Si:2.72 Å, Ob:3.15 Å.

The outer surface was taken to be the basal oxygen plane of the silica tetrahedra on the tenuous evidence of Figures 4 and 5, which can be interpreted as showing this configuration. The continuous Fourier Transform was calculated at intervals of 0.01 $Å^{-1}$ in 3 perpendicular directions corresponding to x^*, y^* and [001]. The intensities, corrected by the Lp factor for a powder, were summed over intervals of 0.1 °2θ, and the resulting sums smoothed by averaging over ±0.2 °2θ for each data point. Calculations were performed for a single-layer cap, and for caps of 2, 3, 4 and 5 layers. Figure 11 shows the comparison between observed and calculated patterns for a 4-layer model. There is general agreement of position and intensity for the observed and calculated patterns, but not in the delineation of the 00*l* peaks. The clarity of 001, 002 and 003 (at about 38 °2θ) in the calculated pattern arises because of the use of a specific model having 4 concentric shells. In reality, hisingerite is made up of spheres, caps and curved layers of various shell thicknesses, and combining these would broaden and lower 00*l* relative to the *hk* reflections.

DISCUSSION

The chemical, TEM and XRD results strongly suggest that hisingerite is a 1:1 ferric layer silicate, with

Table 4. Hisingerite XRD data (*d*-values in Å and interpreted indices).

Indices:	001	02, 11	002	20, 13	04, 22	31, 15	06, 33	40, 26	42, 17
Locality									
Riddarhyttan	7.70	4.44	3.57	2.56	2.26	1.69	1.54		
Gillinge	7.51	4.41	3.58	2.57	2.41	1.68	1.54	1.32	
Solberg	7.65	4.37	3.60	2.57	2.24	1.67	1.57	1.34	
Broken Hill	7.74	4.59	3.53	2.57	2.34	1.70	1.54	1.32	
Canby	7.50	4.40	3.50	2.56		1.70	1.53	1.30	
School House		4.40	3.30	2.56	2.18	1.69	1.53	1.31	
Bellevue King		4.41	3.50	2.56		1.71	1.53	1.38	1.34

https://doi.org/10.1346/CCMN.1998.0460404 Published online by Cambridge University Press

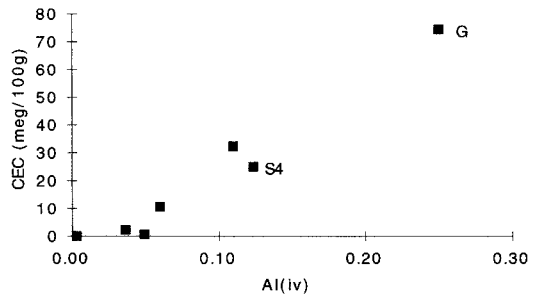

Figure 8. CECs and inferred tetrahedral Al per 2 tetrahedral sites for hisingerites. G: Shayan (1984), S4: Lindqvist and Jansson (1962).

a morphology akin to that of spherical halloysite but of smaller diameter. Its physical properties, particularly its hardness, luster and fracture, are very like those of some halloysites, described by Ross and Kerr (1934) as dense, nonporous and porcelainlike with conchoidal fracture. The TEM images appear to show an interconnected fabric of spheres, caps and curved layers, and the physical properties could perhaps arise from the linkages between these short lengths of normal 1:1 layer silicate structure. Alternatively, the structure could be modulated, with the tetrahedral sheet showing periodic or aperiodic tetrahedral inversions, leading to strong bonding between adjacent layers. The highest-resolution images do not appear to show tetrahedral inversions, but experience imaging ferrous layer silicates such as minnesotaite and greenalite recommends caution in accepting lack of image detail as convincing evidence. In other layer silicates, modulation is associated with planar layers (Guggenheim and Eggleton 1987); thus, the spherical nature of hisingerite is further evidence that the layers are not symmetric across the octahedral sheet, and therefore not modulated.

There is little evidence for a smectite structure in the TEM images of any sample examined other than Bellevue King and Canby. The wavy and straight segments of all samples appear similar to smectite fabrics, but where the layer structure or fringes have been imaged, in all but the Bellevue King and Canby material the repeat unit is at 7 Å and the layers have 2 sheets of slightly different contrast. Collapsed (10-Å) smectites typically show 3-sheet 10-Å layers, and these have only been seen (together with 7-Å layers) in Bellevue King and Canby hisingerite.

On the basis of similarity to the XRD pattern of nontronite, the 7.4-Å peak and the commonly reported 3.6-Å peak may be interpreted as the second and fourth order reflections from a 2:2 layer silicate, but equally they could be the first and second orders from a 1:1 layer. The remaining peaks fit well, but not exactly, to *hk* reflections from a disordered layer silicate having b = 9.23 Å. It is particularly noticeable that

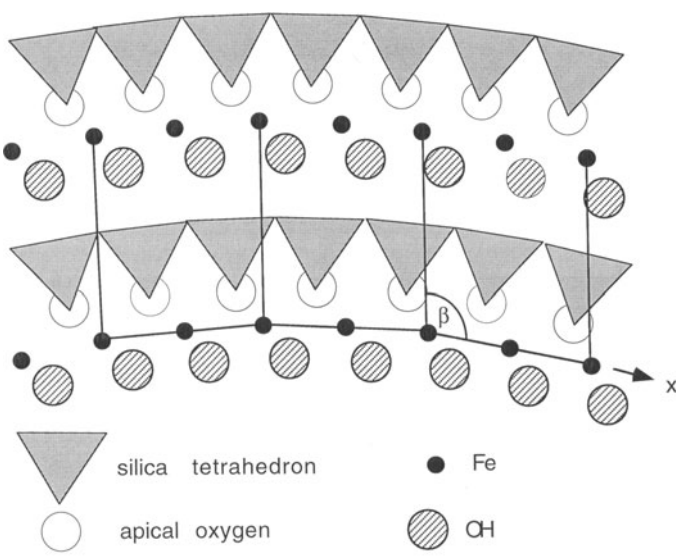

Figure 9. Change in unit cell angle β for a curved crystal. Similar variation occurs for α. Triangles = silica tetrahedra, open circles = apical oxygens and octahedral anions, shaded circles = octahedral OH, small circles = Fe.

https://doi.org/10.1346/CCMN.1998.0460404 Published online by Cambridge University Press

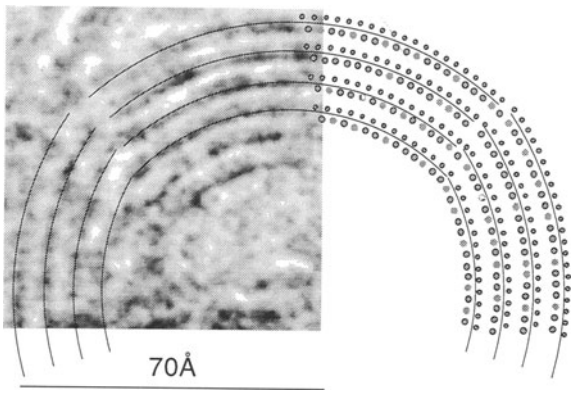

Figure 10. Four spherical caps of ferric kaolinite with radius of curvature 70 Å; YZ section, compared to a TEM image of hisingerite. Larger dots = Fe, smaller dots = Si.

Table 5. Atomic coordinates used for hisingerite XRD calculation. a = 5.37 Å, b = 9.3 Å, $d(001)$ = 7.03 Å.

	x	y	z
Fe1	0	0.333	0
Fe2	0	0.666	0
Si1	0.833	0.167	0.4
Si2	0.833	0.5	0.4
OH1	−0.833	0	−0.16
OH2	−0.833	0.333	−0.16
OH3	−0.833	0.667	−0.16
OA1	0.833	0.167	0.16
OA2	0.833	0.5	0.16
OH6	0.833	0.833	0.16
OB1	0.583	0.083	0.49
OB2	0.583	0.583	0.49
OB3	0.833	0.333	0.49

the 02,11 peak is at approximately 4.43 Å rather than at the value of 4.62 Å predicted from the mean 06,33 spacing of 1.54 Å. The background to the XRD traces below 10 °2θ is very high, presumably resulting from scattering from the spheres and small crystallites. There is a very broad 15-Å peak in the Bellevue King sample, but none is evident in the Riddarhyttan, Gillinge, "Solberg" or Broken Hill samples. However, since TEM images show very few coherent layer sequences except within the 7-Å layer spheres, a 14-Å peak, should it be present, would be weak and broad. We conclude that there is little XRD evidence for hisingerite being a poorly crystallized form of nontronite, but we do not regard the XRD results alone to be definitive.

The calculated XRD pattern of the spherical ferric-kaolin model fits the observed data better, in d-values, intensity and line profile, than calculated patterns based on a normal crystallographic lattice. All the hk peaks that have hitherto been regarded as evidence for poorly crystalline nontronite are reproduced by this model calculation, but in positions closer to those observed for hisingerite than those of nontronite.

The chemical analyses of hisingerites show little to no Al : Si substitution (none in the Gillinge sample, at most 0.05 per 2 tetrahedral sites in Riddarhyttan and "Solberg" material). This compares with zero tetra-

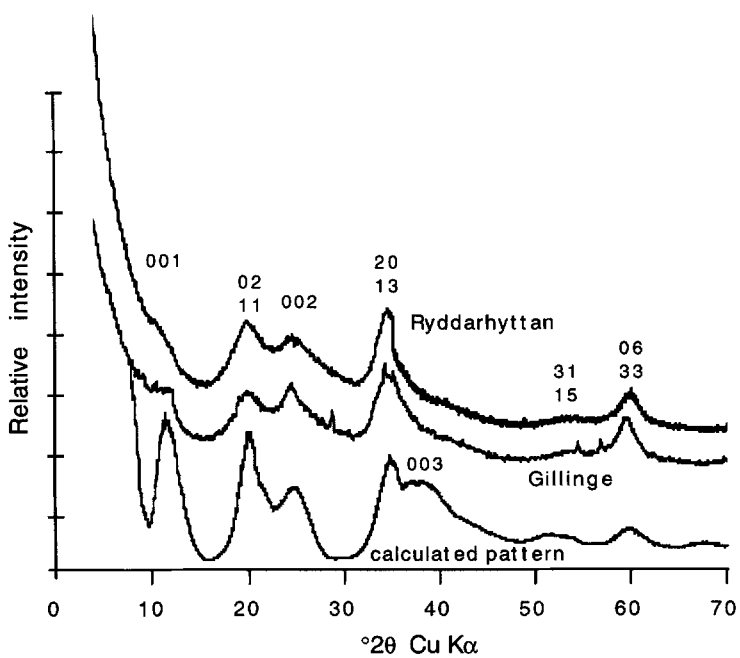

Figure 11. Observed and calculated XRD scans for hisingerite (Cu$K\alpha$).

https://doi.org/10.1346/CCMN.1998.0460404 Published online by Cambridge University Press

hedral Al in kaolinite and halloysite, but not with typical values of 0.22 per 2 tetrahedral sites found in nontronites (Brigatti 1981).

CEC results are further evidence that hisingerite is not poorly crystallized nontronite. Smectites typically have CECs of 100 meq/100 g or greater, whereas type hisingerite has a CEC of 2 meq/100 g. There is TEM and XRD evidence that the Bellevue King sample includes some 2:1 layers, and the high CEC (32 meq/100 g), and Si + Al > Fe + Mn + Mg is consistent with a mixture of smectite and hisingerite. The close correlation between the Al (assumed tetrahedral) and CEC can be interpreted as showing the amount of nontronite in the hisingerite samples—none for Gillinge and Riddarhyttan, perhaps 30% for Bellevue King and a great deal for the Geeolong sample.

Some of the hisingerites analyzed here have more water evolved above 100 °C than can be accommodated in a kaolin-like formula, and halloysite behaves similarly in this regard (Brindley and Goodyear 1948). Water trapped inside the spheres may not be completely lost by the time a typical heating analysis experiment has passed 100 °C. The nature of the OH loss from hisingerite is different from that reported from other layer silicates, in that the bulk is lost below 400 °C, some 100 °C lower than for halloysite. This may result from the very poorly organized structure, allowing easy breakdown during heating. The hygroscopic character of hisingerite appears to be a consequence of its very large specific surface area, which by calculation on the basis of 3-layer spheres of internal radius 50 Å and external radius 70 Å have a total surface area of the order of 250 m^2/g. The measured density is in accord; a sphere of this size having ferric halloysite composition has a calculated density of 2.4 g/mL.

It is apparent that there is either more than 1 hisingerite-like material from Gillinge and Solberg, or that earlier analyses were performed on incompletely purified material, or that some labels have been inadvertently exchanged—or all 3 sources of confusion exist. Table 3 summarizes the data relating to this point. Hisinger's description of the "black species of stone from Gillinge" fits our sample 070080, but his analysis differs markedly from all others in having much more Al_2O_3 and Fe_2O_3. Sample SMNH 48-1817 from Gillinge, which was not studied in detail, has a composition similar to SMNH 070080 (Table 3). The material analyzed by Mackenzie and Berezowski (1980) from the Gillinge Mine (Uppsala University collection gillingite 400/4) is very manganiferous, and was reported as neotocite by Lindqvist and Jansson (1962, Sample MGIU 400/4). Our sample SMNH 400/2 from Solberg is also manganiferous, whereas Mackenzie and Berezowski's analysis of Solberg material (Uppsala University collection 400/2) lacks Mn and closely matches analyses of Gillinge hisingerite reported by Cleve and Nordenskiöld (1866) as well as those reported here. It seems probable that the sample we have examined said to be from Solberg (MGIU 400/2) is actually another Gillinge sample, possibly MGIU 400/4. Our conclusions concerning hisingerite from Gillinge are based on sample 070080; our results on MGIU 400/2, no matter whence it came, are corroborative evidence of the earlier findings (Eggleton et al. 1983) that Mn-bearing hisingerites are comparable to Fe-hisingerite.

The composition of type hisingerite (Riddarhyttan) is $Al_{0.04}Fe_{1.88}Mg_{0.06}Si_{2.03}O_5(OH)_4$ calculated to +14. If Al is tetrahedral, the tetrahedral : octahedral cation ratio is 2.07:1.92, whereas if Al is octahedral, the ratio is 2.03:1.98. The CEC evidence and the composition of Gillinge hisingerite indicate that tetrahedral Al is minimal in hisingerite, and that to within experimental error the tetrahedral octahedral ratio is 1:1. All the evidence presented here compels the recognition that hisingerite is a new ferric-iron member of the kaolin group of minerals.

ACKNOWLEDGMENTS

D. Holtstam of the Swedish Museum of Natural History kindly provided the Riddarhyttan and Gillinge samples, as well as giving great assistance in sourcing the original literature. The ANU's Electron Microscope Unit provided SEM and TEM facilities. This research has been supported under the Australian Government's Cooperative Research Centres Program.

REFERENCES

Archimedes. ca 250 BC. On floating bodies, Book I.

Berzelius J J. 1819. Nouveau systeme de minéralogie. Paris: Méquignon-Marvis. 314 p.

Bowie SHU. 1955. Thucolite and hisingerite-pitchblende complexes from Nicholson Mine, Saskatchewan, Canada. Bull Geol Surv Gr Brit 10:45–55.

Brigatti MF. 1981. Hisingerite: A review of its crystal chemistry. Proc 7th Int Clay Conf. Dev Sedimentol 35:97–110.

Brindley GW, Goodyear J. 1948. X-ray studies of halloysite and metahalloysite. II. The transition of halloysite to metahalloysite in relation to relative humidity. Mineral Mag 28:203–215.

Church MA. 1870. Chemical researches on new and rare Cornish minerals. J Chem Soc 23:3–5.

Churchman GJ, Slade PG, Self PG, Janik LJ. 1994. Nature of interstratified kaolin-smectites in some Australian soils. Aust J Soil Res 32:805–822.

Cleve PT, Nordenskiöld AE. 1866. Om sammansättningen af jernhaltige kolloïd-silikater. Öfversigt af Kongl. Vetenskaps-Akademiens Förhandlinger 237:169–183.

Cowley JM. 1961. Diffraction intensities from bent crystals. Acta Crystallogr 14:920–927.

Dietrich RV. 1961. Contributions to the mineralogy of Norway 12. Hisingerite in "dark" larvikite. Norsk Geologisk Tidsskrift 41:95–108.

Eggleton RA. 1987. Noncrystalline Fe-Si-Al oxyhydroxides. Clays Clay Miner 35:29–37.

Eggleton RA, Pennington JH, Freeman RS, Threadgold IM. 1983. Structural aspects of the hisingerite-neotocite series. Clay Miner 18:21–31.

Gordon SG. 1944. The mineralogy of the tin mines of Cerro de Llallagua, Bolivia. Proc Acad Nat Sci Phila 96:355. (Note that Bowie [1955] incorrectly referenced this as published in volume 66, 1934.)

Gruner JW. 1935. The structural relationships of nontronite and montmorillonite. Am Mineral 20:475–483.
Guggenheim S, Eggleton RA. 1987. Modulated 2:1 layer silicates: Review, systematics, and predictions. Am Mineral 72:724–738.
Hawkins AC, Shannon EV. 1924. Canbyite, a new mineral. Am Mineral 9:1–5.
Hewett DF, Schaller WT. 1925. Hisingerite from Blaine Co., Idaho. Am J Sci 210:29–38.
Hisinger W. 1810. Undersökning af Svenska Mineralier. VI. Svart Stenart från Gillinge Jern-Grufva i Södermanland. Afhandlingar i Fysik, Kemi, och Mineralogi 3:304–306.
Hisinger W. 1826. Versuch einer mineralogischen Geographie von Schweden. Barth JA, Leipzig.
Hisinger W. 1828. Analyse des mit dem Namen Hisingerit belegten Eisensilicats. Annalen der Physik und Chemie von J.C. Poggendorff Bd 13:505–508.
Kohyama N, Sudo T. 1975. Hisingerite occurring as a weathering product of iron-rich saponite. Clays Clay Miner 23: 215–218.
Lindqvist B, Jansson S. 1962. On the crystal chemistry of hisingerite. Am Mineral 47:1356–1362.
MacEwan DMC 1951. In: Bradley GW, editor. X-ray identification and crystal structures of clay minerals (first edition). London: Mineral Soc.
MacEwan DMC. 1961. In: Brown G, Brindley GW, editors. The X-ray identification and crystal structures of clay minerals (second edition). London: Mineral Soc.
Mackenzie KJD, Berezowski RM. 1980. Thermal and Mössbauer studies of iron-containing hydrous silicates: II. Hisingerite. Thermoc Acta 4:335–355.
Manceau A, Ildefonse Ph, Hazemann JL, Flank A-M, Gallup D. 1995. Crystal chemistry of hydrous iron silicate scale deposits at the Salton Sea geothermal field. Clays Clay Miner 43:304–317.
Mohs F. 1839. Leichtfassliche Anfangsgründe der Naturgeschichte des Mineralreichs. Wien: Carl Gerold.
Muir ID. 1954. Crystallization of pyroxenes in an iron-rich diabase from Minnesota. Mineral Mag 30:376–388.
Osborne FF, Archambault M. 1950. Hisingerite from Montauban-Ies-Mines. Le Naturaliste Canadien 77:283–290.
Rammelsberg C. 1848. Ueber die Zusammensetzung des Hisingerits. Annalen der Physik und Chemie 75:398–402.
Ross CS, Kerr PF. 1934. Halloysite and Allophane. USGS Prof Pap 185-G:135–148.
Schwartz GM. 1924. On the nature and origin of hisingerite from Parry Sound, Ontario. Am Mineral 7:141–144.
Shayan A. 1984. Hisingerite material from a basalt quarry near Geelong, Victoria, Australia. Clays Clay Miner 32: 272–278.
Simpson ES. 1918–19. Hisingerite. J Proc R Soc W Aust 5: 95–97.
Sudo T, Nakamura T. 1952. Hisingerite from Japan. Am Mineral 37:618–621.
Sustschinsky PP. 1910. Über den Hisingerit. Zeit Kryst u Mineral 47:231–237.
von Kobell Fr. 1828. Ueber das Eisensilicat von Bodenmais (Thraulit). Annalen der Physik und Chemie von J.C. Poggendorff Bd 14:467–469.
Whelan JA, Goldich SS. 1961. New data for hisingerite and neotocite. Am Mineral 46:1412–1423.

(Received 8 January 1997; accepted 5 November 1997; Ms. 97-005)